Development of Tensile Split Hopkinson Pressure Bar Technique for Studying the Dynamic Behaviour of Metals

Mohammad Mohsin Khan[a],*, Ajay Kumar[a],**, and Mohd Ashraf Iqbal[a],***

[a] Civil Engineering Department, Indian Institute of Technology Roorkee,
Roorkee, 247667 India
* e-mail: mkhan@ce.iitr.ac.in
** e-mail: ajay.ce@sric.iitr.ac.in
*** e-mail: iqbalfce@iitr.ac.in

Abstract—The tensile split-Hopkinson pressure bar (SHPB) system is significantly used for dynamic material characterization of metals in the range of strain rates 10^2–$10^4\,\mathrm{s}^{-1}$. There is no standard design methodology or readily available technique for the development of this apparatus. In the present study, a detailed design and development of tensile SHPB apparatus for dynamic material characterization of metals in tension has been presented. The output incident and transmitted wave signals obtained were found to be consistent with the striker bar impact velocity that was varied in the range 4–14 m/s and the wave speed in the steel 4340 bar observed as 5144 m/s. The elastic compressive wave generated in incident bar, which was effectively transmitted to the transmission bar through the shoulder. This process showcased the high accuracy and precision of the bar alignment system, along with the parallel alignment of the bar end faces. To avoid the disturbance caused by the shoulder in the output bar, the length of the output bar and input bar were set to 2000 and 1500 mm, respectively. Furthermore, positioning SG-2 along the output bar and SG-3 along the input bar was found the most optimal position to avoid disturbances in the output signals.

The average experimental incident wave strain peak amplitude (Average of strain at SG-1 and SG-2) recorded at 4.1, 5.95, 8.3, 10.3, and 12.5 m/s striker impact velocity was −405, −588, −815, −1014, and −1243 micro-strain, respectively. It was observed −1.69, −1.76, −1.03, −1.36, and −2.37% error in the incident wave strain amplitude at the respective impact velocities. Similarly for the proper alignment of Striker, incident, shoulder, and transmission bar, the average values of the recorded strain gauges have 1.80, 1.93, 1.43, 1.26 and 1.70% higher strain amplitude as compared to analytical values corresponding to their striker impact velocities. Based on experimental results, it has been observed there were less than 2.5% error was observed in the average peak strain in comparison to the analytical results. Hence, it has been concluded that the system is accurately aligned such that in the absence of a specimen the striker, incident, shoulder, and transmission bars function as a single bar. It may be concluded that the developed SHPB-T setup has been well calibrated and could be suitably used to perform the further experiments on metals.

Keywords: tensile split hopkinson pressure bar, loading components, bar components, data acquisition and recording system, wave characteristics and calibration

DOI: 10.3103/S0025654423601568

1. INTRODUCTION

The brittle and ductile materials like concrete, metals and composite are significantly experience the dynamic loading conditions in their service life. Hence, the researcher is continuously working on the determination of material properties and their response under the high rate of deformation conditions. The material characteristic and failure mechanism under high rate of loading conditions are drastically different from those quasi-static loading conditions. The dynamic characteristics of ductile and brittle materials have wider utilization in the structural, aerospace, military, power generation and defense applications. Therefore, it's very essential to investigate the material properties and failure response subjected to high rate of loading for analysis and design of the structures for their security and safety purposes.

The various sophisticated experimental techniques have been developed in the past to investigate the dynamic material properties. The servo-hydraulic machine used to generate the quasi-static loading con-

ditions up to 10^{-2} s^{-1} strain rate and neglected the inertia effect, but the obtained data is too noisy [1]. In addition, the Drop weigh Hammer test used to generate the intermediate strain rate 10^{-1} to 10^1 s^{-1} and it have wider application to simulate the earthquake and vehicle impact condition where inertia play a significant role, but the loading conditions are no well controlled as the hammer direct impact on the materials [2, 3]. To generate the high rate of loading conditions, the split Hopkinsion pressure bar test (SHPB) and pneumatic gun test were used. The strain rate developed are in the range of 10^1 to 10^4 s^{-1} and significantly used to generate the rock blasting, bullet impact and dynamic explosion situations. Whereas, the debris impact on spacecrafts and nuclear explosive conditions are generated by the two-stage light gas gun, plate impact test and Taylor impact test. The strain rates are very high varied in the range of 10^4 to 10^6 s^{-1} and the inertia play a crucial role in the material response. Events that produce high strain rates, whether they arise from human activities or natural occurrences, exceed the proficiencies of hydraulic machines, and drop weight hammer tests. In these scenarios, the effects of inertia and wave propagation play a significant role, particularly when subjected to high strain rate loads ranging from 10^1 to 10^4 s^{-1}. The SHPB technique has gained popularity to anticipate how both brittle and ductile materials respond dynamically to deformation. The foundational concepts, fundamental principles, setup guidelines, experimental procedures, and wave analysis techniques for SHPB application on both brittle and ductile materials have been comprehensively elucidated by Cheng et al. and Grey III [2, 4].

The split Hopkinson Pressure Bar setup widely used to determine the dynamic material properties of steel, aluminium, iron, and copper. These ductile materials have valuable practical application in the field of material science and engineering for safety and security purposes. The SHPB tests can provide information on the dynamic behavior of steels and aluminium alloys, such as its strength, stiffness, and ductility under high strain rates [5, 6]. This information is critical for material selection and design in industries like aerospace, automotive, and civil engineering. Researchers can use SHPB to study the behavior of ductile materials under extreme conditions, helping to advance the development of new materials with improved properties [7, 8].

Understanding the dynamic behaviour of steel and aluminium subjected to dynamic loads is essential for analysis and designing the critical infrastructures and vehicles that can withstand impact, blast, and crash events. Hence, SHPB data can be used to improve the safety of automobiles, aircraft, and other transportation systems. Steel and aluminium alloys is commonly used in the construction of armor, such as body armor, vehicle armor, and fortifications. SHPB tests help in evaluating the steel's ability to resist high-velocity projectiles and explosions, aiding in the development of effective armor materials [5, 6]. Ductile materials are used in various defense applications, and understanding its dynamic behavior is essential for developing weapons, protective gear, and military equipment. Aircraft and spacecraft components are often subjected to dynamic loads during launch, re-entry, and other mission phases. SHPB data can help in designing materials and structures that can withstand these loads [9−12].

The dynamic mechanical properties of ductile materials i.e., steel, aluminium, copper, iron etc. obtained through SHPB tests are essential for ensuring the safety and reliability of various systems and structures subjected to high-velocity impacts, vibrations, and other dynamic forces. These applications demonstrate the significance of such research in a wide range of fields including the material science, engineering, and material characterization. Hence, design, development, and calibration of SHPB setup to investigate the dynamic tensile properties of ductile materials in the range of 10^2 to 10^4 s^{-1} strain rate become very essential.

1.1. Historical Overview of SHPB Apparatus

In 1872, J. Hopkinson firstly conducted the dynamic test by dropping the weight on the metallic wire and concluded that the rupturing occurred either at impact location or at the fixed end depends upon impact speed irrespective of the mass of weight. The concept of wave propagation reveled but not measured due to lack of measurement technique [13, 14]. Later, in 1914, B. Hopkinson measured the pressure-time response of stress wave in the pressure bar generated due to explosion and bullet impact but the curve was approximate due to limited measurement [15]. Davis [16] introduced a method based on the electrical measurement of lateral and radial displacement of the bar end and cylindrical surface with the time.

Kolsky [17] was the first person who used the concept of indirect impact loading on the testing material. The testing specimen has been sandwiched between the two-silver steel bar called as pressure bar and the pressure and displacement time response in the pressure bar measured by using the electrical condenser microphone as proposed by the Davis [16]. The recorded pressure-time and displacement -time response in the pressure bar used to determine the stress-strain response of the tested material under dynamic conditions. Kolsky technique conducted a series of experiments on a range of materials including

rubbers (natural and synthetic), metals and polyethylene. These tests resulted in a notably improved understanding of the dynamic stress-strain behavior exhibited by these materials. The stress wave propagation measuring technique widely adopted during the initial several years. Later in 1954, the Kraft et al. [18] replaced the electrical condense microphone with the electrical resistance strain gauge to measure the stress wave in the pressure bar and this technique become a standard method for the Kolsky bar tests. Kraft et al. additionally substituted the bullet or detonator with a loading projectile, termed the "striker bar," in order to create a consistent, control and repeatable trapezoidal-shaped pulse. Before 1960, the Kolsky tests were used only to study the dynamic compression properties of ductile and brittle materials.

In 1960, Harding et al. [19] firstly used the Kolsky setup for the dynamic tensile loading condition. Kolsky bar configuration was adjusted to induce a dynamic tensile loading scenario through a variation in the loading technique, while keeping the fundamental principles of wave propagation theory intact. Through these modifications, Harding et al. [19] achieved the accurate stress-strain depiction of ductile materials under tension at a strain rate of 1000 s^{-1}. In 1966, Hauser and Frank [20] conducted a comprehensive examination of experimental methodologies employed under dynamic loading circumstances. They successfully enhanced the precision and accuracy of stress-strain, strain rate, and strain correlations by overcoming the challenges that had previously hampered such investigations.

Later in 1972, the SHPB technique has been extended by the Duffy et al. [21] for the torsional loading condition and concluded as the best experimental method for the torsional loading during that time and the results were explained for 1100-O aluminum alloy in at the 800 s^{-1} strain rate. Subsequently, many researchers and investigators have suggested various modifications to the Kolsky bar setup to enhance the accuracy of stress-strain responses for materials under different loads. [16−18]. In 1972, Duffy et al. [21] extended upon the SHPB technique to incorporate the torsional loading conditions without changing the basic concept and working principle of SHPB. Their work determined the SHPB technique as the most effective experimental approach for torsional loading. The results they obtained were specifically explained for the 1100-O aluminum alloy, tested at 800 s^{-1} strain rate. Following this, numerous researchers suggested several enhancements to the Kolsky bar setup in order to enhance the precision of stress-strain analysis for materials subjected to various loading circumstances [22−24].

Throughout the 20th century, the SHPB apparatus found application in applying various loading conditions to materials. These dynamic loading conditions obtained by changing the specimen gripping technique to generate the compressive, tensile, torsional, and bending loads without disturbed the basis working principle of SHPB apparatus. Still the basic design setup of SHPB remained unchanged. In 2009, Song et al. [25] accepted a redesign of the Kolsky bar compression setup, incorporating advanced modifications to meet the requirements of mechanical analysis of materials subjected to high strain rates. Illustration upon the progress achieved by multiple researchers in refining the original SHPB configuration, the most recent iteration, depicted schematically in Fig. 1, has been universally adopted and deployed for the investigation of dynamic material responses.

While the fundamental structure of the SHPB (Split Hopkinson Pressure Bar) setup remains consistent, there are notable variations in the mechanical components and data acquisition methods. These discrepancies arise from differences in the material under examination, loading circumstances, specimen dimensions, and desired strain rates. As a result, the specific design and construction particulars diverge across laboratories in accordance with the unique investigative demands. The raw experimental data acquired from the split Hopkinson pressure bar (SHPB) setup could exhibit inconsistencies and variations in outcomes when examined in various laboratories for the same material [26]. In the past few decades, there has been a growing need for accurate material characterization, driven by both strategic and economic advancements. However, obtaining the necessary tools for designing, developing, and calibrating split Hopkinson pressure bars (SHPB) for the dynamic characterization of ductile and brittle materials remains a challenging task. The detailed description and geometrical configuration of different components of SHPB and calibration of the developed setup were not presented in the previous literatures.

In this manuscript, our primary aim is to comprehensively explain the intricate process of designing, developing, and calibrating of split Hopkinson pressure bar (SHPB) arrangement for the careful characterization of materials under conditions of elevated strain rate loading. The comprehensive explanation of the fundamental operating principles and essential theoretical foundations required for developing an SHPB setup has been provided. Furthermore, a detailed discussion has taken place regarding the loading elements, bar constituents, and technical specifics of the data acquisition and quantification system (DAQS). All constituent elements have been methodically integrated, subsequently undergoing a preliminary test to facilitate the precise calibration of the setup. Initial trials were executed in the absence of the specimen, effectively rendering the pressure bars to function as a singular unit. This approach was delib-
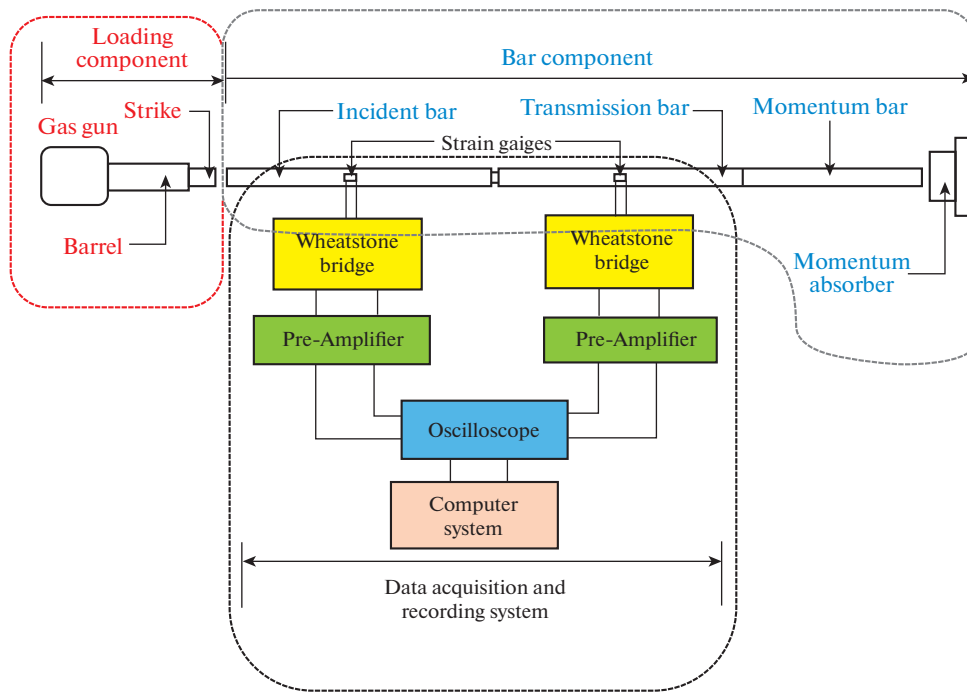
Fig. 1. Schematic of classical SHPB setup.

erately adopted to generate congruent trapezoidal pulses within both the incident and transmission bars, minimizing the occurrence of any discernible reflected pulses or their negligible impact.

2. SPLIT HOPKINSON PRESSURE BAR TEST APPARATUS

2.1. SHPB Test Setup for Tensile Loading

The standard SHPB compression setup has been modified for other types of high rate of loading conditions including tension and torsion SHPB methods. Numerous setups have been developed for producing stress pulses of dynamic tensile loading [19, 24, 27−30]. These approaches can be categorized into two main groups. The first group involves changing the experimental setup to generate the input stress pulse for dynamic tensile loading. The most utilized technique employs a hollow striker bar that moves along the incident bar and strikes the anvil to generated the tensile loading stress pulse in the incident bar. Gerlach et al. [27] used a U-shaped striker bar in place of hollow striker bar to generates the loading pulse in incident bar. The methods in the second category for creating tensile loading pulses involve utilizing the classical split Hopkinson pressure bar (SHPB) Compression setup. In these approaches, specimens are designed with specific shapes, such as an M-shaped specimen [28] or a dumbbell shaped threaded specimen with a split shoulder or collar [24]. These methods have the advantage of simply adapting a standard compression SHPB system to a configuration that allows for testing materials under uniaxial tensile stress dynamic conditions. Among these methods, a straightforward option appears to be the SHPB variation incorporating a shoulder design.

In this testing approach, the initial incident and transmission stress pulse (compressive in nature) observed like the classical SHPB compression method. The compressive stress pulse generated in incident bar by striker impact traverses through the shoulder's cross-section, the specimen, and the transmission bar. Subsequently, this compressive stress pulse reflected and travel back in the transmission bar as the tensile stress wave. This tensile stress pulse is partly absorbed by the specimen and partly reflected due to the difference in the mechanical impedance $\left(Z = \dfrac{F}{V} = A\rho C_o \right)$ of bar material and specimen material. Notably, the shoulder plays no role in transmitting the tensile stress pulse in the incident bar as it has no contact with the incident bar. This intricate process involving the transmitted and reflected pulses provides valuable insights essential for characterizing the material's constitutive behavior. The shoulder is fabricated from the identical material as the incident and transmission bar with the same outer diameter. The
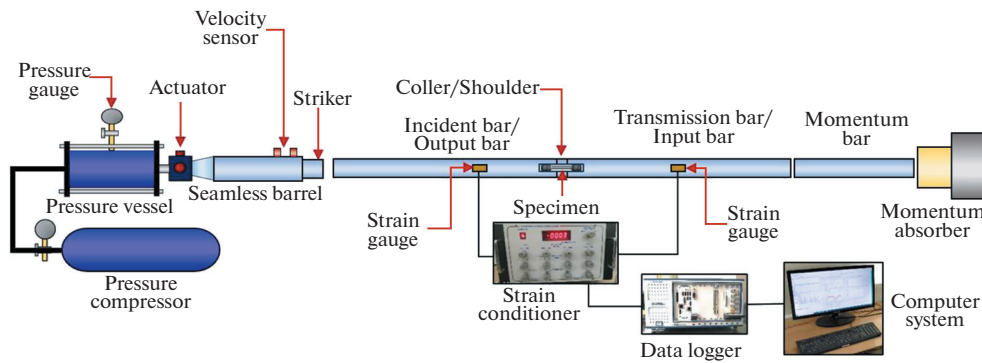
Fig. 2. Schematic diagram of developed SHPB for tension.
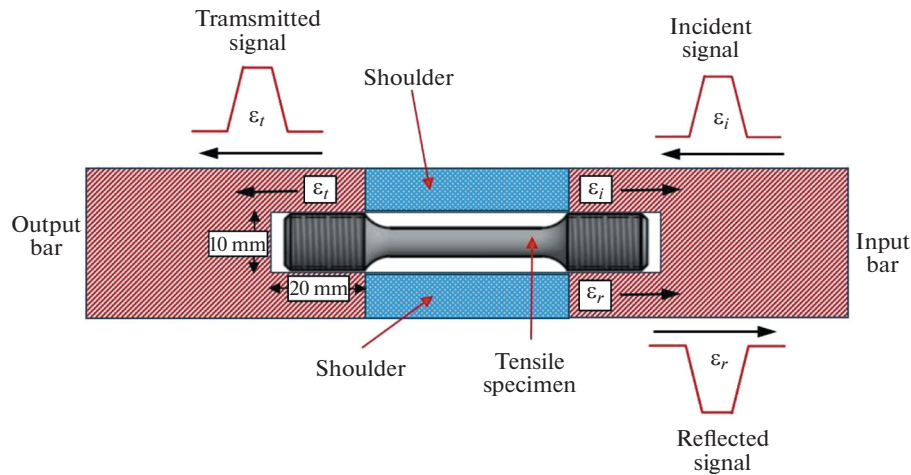

Fig. 3. Schematic of stress wave propagation in input and output bars.

internal diameter of the shoulder is generously sized to accommodate the specimen without any physical contact. The shoulder's cross-sectional area substantially exceeds that of the specimen, and its outer surface is meticulously aligned parallel to the bar ends. The shoulder must be in proper end to end contact with the incident and transmission bar to properly transmitted the loading stress pulse. The incident stress pulse (compressive), transmitted stress pulse (compressive) and reflected stress pulse (tensile) were recorded by the strain gauge mounted at the outer surfaces of the incident and transmission bar with the help of (DAQS). The schematics diagram of the developed SHPB for tension has been shown in Fig. 2. Drawing upon the principles of SHPB theory, and in consideration of stress pulse transmission, the authors have revised the nomenclature of the bars. Specifically, the transmission bar facilitating the propagation of the first useful tensile stress wave, is now termed the "input bar," while the other bar (Incident bar) is referred to as the "output bar." In the case of the SHPB-T method involving a shoulder method for tensile loading condition, both the compression pulse and the transmitted pulse travel through the output bar. The revised nomenclature of bars and wave propagation in the SHPB-T has been shown in Fig. 3.

2.2. Working Principle and Equations

The SHPB-T setup similarly worked on the principal of classical SHPB method but the only difference in the specimen gripping method. In SHPB-T, the dumbbell shaped specimen has been screwed in between input and output bar, see Fig. 3. The shoulder placed to encased the specimen for the transmission of compressive stress pulse. The input, output, shoulder, and striker bar must be remaining linear elastic and centric during the entire loading process. The generated elastic wave should have one-dimensional wave propagation behaviour. The specimen deformation should be uniform and followed the equilibrium condition during failure process. The strain associated with incident signal, reflected signal, and

transmitted signal are referred as the ε_I, ε_R, and ε_T, respectively, see Fig. 3. These strain values linked with the incident wave, reflected wave, and transmitted pulse waves are then utilized to ascertain the relationships between stress, strain, and strain rate-time response with in the testing specimen.

Based on the concept of 1D elastic wave propagation theory and hook's law, the stress, strain, and strain rate in the specimen are obtained by the following equation;

$$\sigma_c(t) = E_b\left(\frac{2A_b}{A_s}\right)(\varepsilon_I + \varepsilon_R + \varepsilon_T), \tag{1}$$

$$\varepsilon_c(t) = \frac{C_o}{L_o}\int_0^t (\varepsilon_I - \varepsilon_R - \varepsilon_T)dt, \tag{2}$$

$$\dot{\varepsilon}_c(t) = \frac{C_o}{L_o}(\varepsilon_I - \varepsilon_R - \varepsilon_T). \tag{3}$$

If specimen is in equilibrium and the bars have same material properties with equal cross sectional then

$$\begin{bmatrix} (\varepsilon_I + \varepsilon_R = \varepsilon_T) \\ Equilibrium Condition \end{bmatrix}. \tag{4}$$

Therefore, the Eqs. 1, 2, and 3 modified as;

$$\sigma_c(t) = E_b\left(\frac{A_b}{A_s}\right)\varepsilon_T, \tag{5}$$

$$\varepsilon_c(t) = -\frac{2C_o}{L_o}\int_0^t \varepsilon_R dt, \tag{6}$$

$$\dot{\varepsilon}_c(t) = -\frac{2C_o}{L_o}\varepsilon_R, \tag{7}$$

where $\sigma_c(t)$, $\varepsilon_c(t)$, and $\dot{\varepsilon}_c(t)$ are the stress, strain, and strain rate time histories in the specimen, respectively. A_b and A_s are the cross-sectional areas of bar and specimen, respectively. C_o and L_o are elastic wave speed in bar and initial length of specimen, respectively.

3. LOADING SYSTEM

3.1. Configuration of Pneumatic Gun

The pneumatic gas gun setup also termed as the loading component to generate the stress loading pulse are the assembly of the seamless barrel, velocity sensor, pressure vessel, pressure compressor, actuated ball valve, and pressure regulator. The schematic diagram and real diagram of the pneumatic gas gun have been shown in Figs. 4a and 4b, respectively. The seamless barrel is made up of the mild steel with a length of 1.5 m, outer diameter 32 and 26.5 mm outer diameter. The inner diameter of barrel is more than the diameter of the striker. The two or three hollow cylindrical Teflon tube with a 3 mm thickness was provided over the striker for the following purpose; (i) Smooth movement of striker bar inside the barrel, (ii) Minimize the friction and heat generated between barrel and Teflon tube during propagation of striker bar, and (iii) Prevent the damage of outer surface of the striker bar. The pressure vessel is made up of the EN 28 steel material having the 20 mm thickness of wall and 1 liter capacity. The electrically controlled actuator ball-valve system rapidly released pressure into the seamless hollow cylindrical barrel to accelerate the striker bar. This ball-valve act as a pressure switch, capable of turning the pressure on or off operated at pressures between 5−8 bar, with a maximum allowable pressure of 200 bar. The seamless barrel is connected to the pressure vessel through the actuator ball-valve, as shown in Fig 3.

3.2. Pressure Compressor, Pressure Controller and Velocity Measurement Sensor

The JUNIOR II breathing air compressor (Fig. 5a) generated pressure in the cylindrical vessel. This pressure was regulated using a pressure pipe and regulator (Fig. 5b) connected to the vessel. A pressure gauge was attached to monitor vessel pressure, while impact velocity was determined using metallic sensors (Fig. 5c). These sensors were positioned 100 mm apart near the barrel's end. The striker velocity was
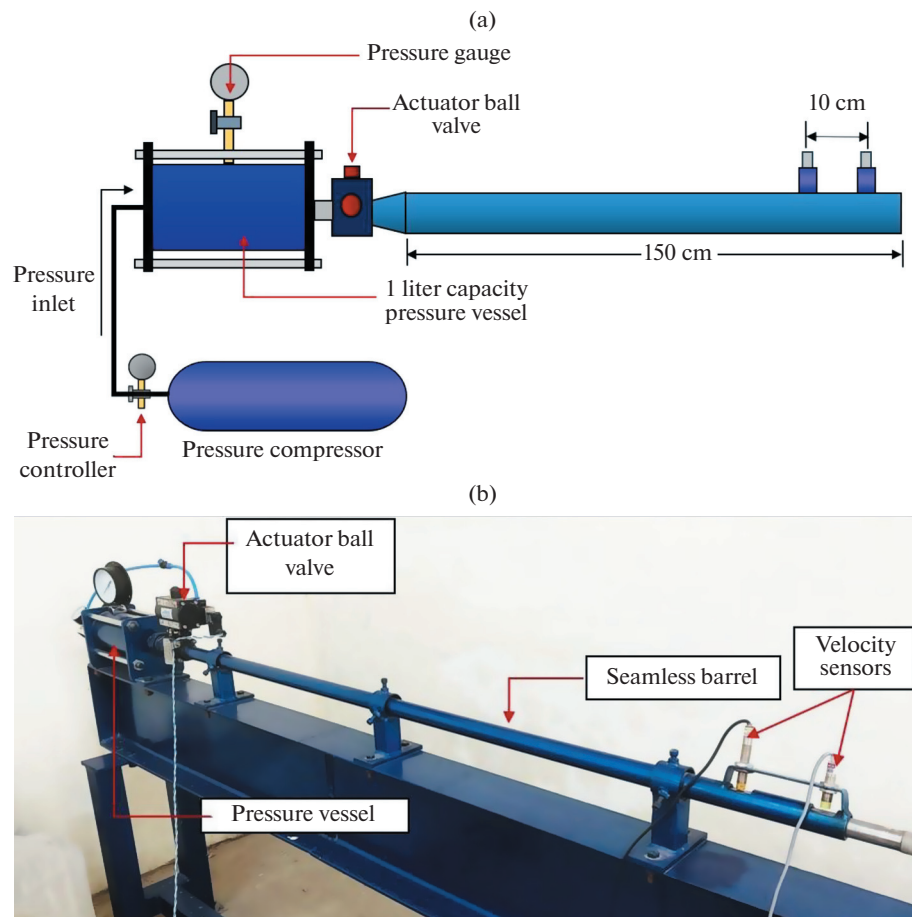
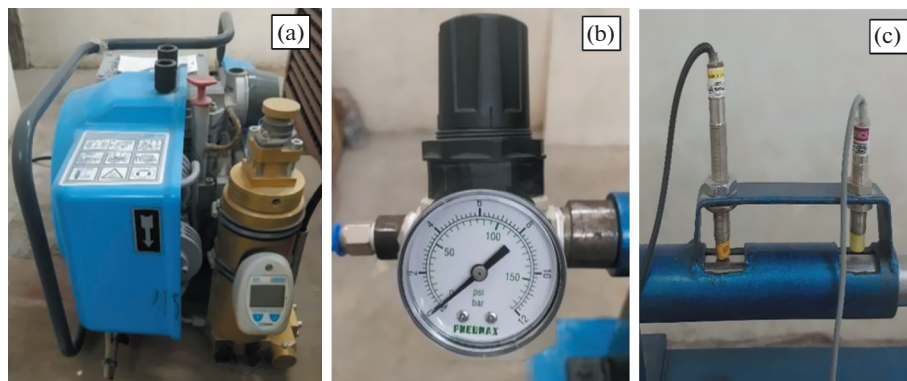**Fig. 4.** (a) Schmetic diagram of pneumatic gas gun. (b) Actual developed gas gun diagram.


Fig. 5. (a) Pressure compressor: (b) Pressure controller: (c) Velocity measurement sensor.

determined by the time it took to move between these sensors, adjustable using the pressure inside the vessel. The striker bar's impact velocity was adjustable by varying vessel pressure and could be measured accurately up to 60 m/s, with a minimum detectable difference of 0.1 m/s. The bar component and the loading component have been placed, positioned, and located over the supporting stand made up of the mild steel square hollow tubular section and grounded through the fasteners. The I-section heavy duty
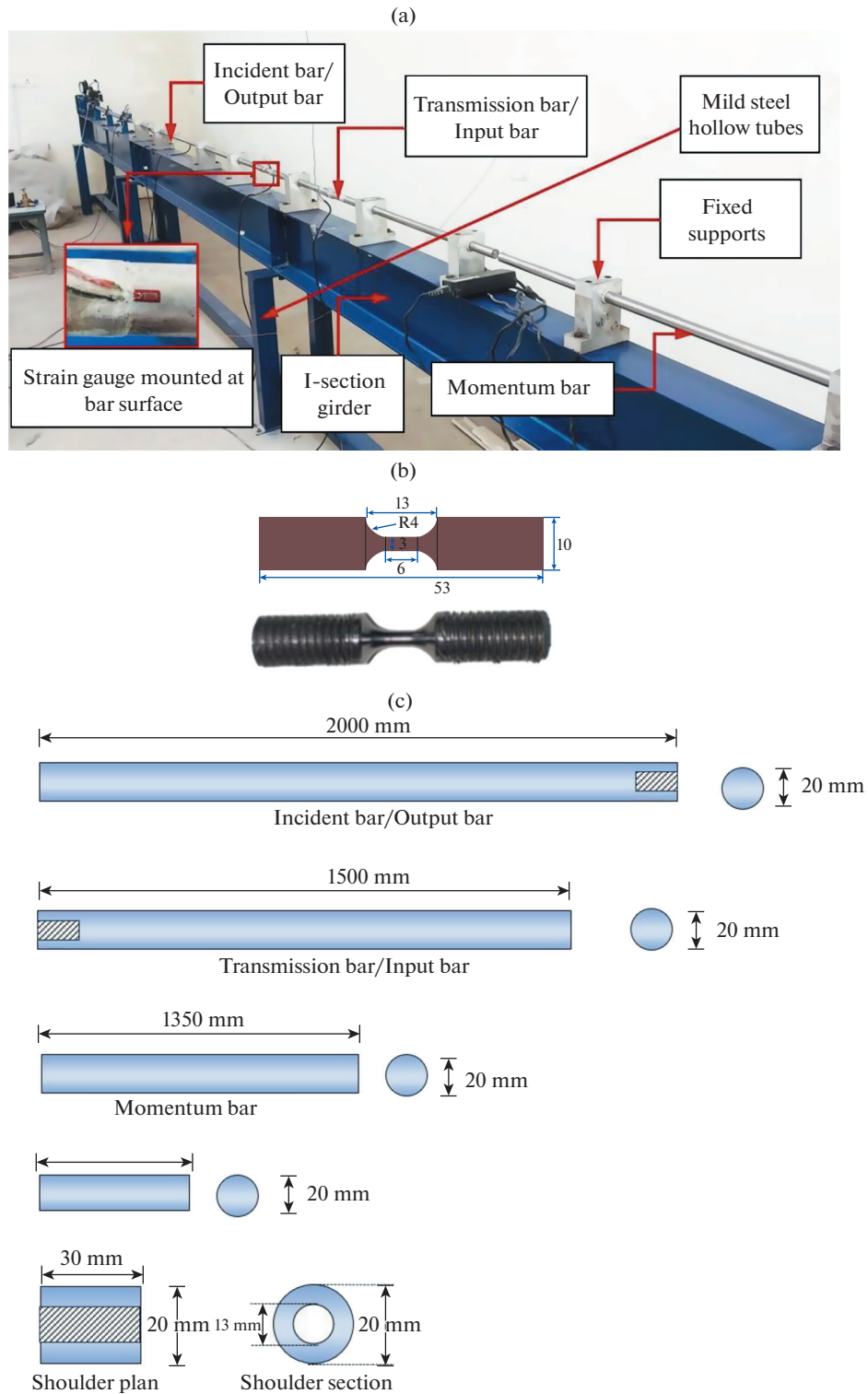
Fig. 6. (a) Schematic of bars components with dimensions. (b). Actual bar components for SHPB-T. (c). Tensile specimen for dynamic loading condition.

steel girder have been placed over the supporting stand. The nine fixed supports directly mounted over the girder to support the incident, transmission, and momentum bar, see Fig. 6b.

4. BAR COMPONENTS OF SHPB-T

The input, output, momentum, and striker bar must be in linear elastic region during dynamic experiments so that the strain on bar surface can be linearly correlated with the stress wave propagating in the input and output bar. Hence the high strength steel preferred to fulfill this requirement. In this study the Steel 4340 bar has been used with higher length to diameter ratio to fulfill the requirement of one-dimensional propagation of stress wave [25]. The strain gauge is positioned a minimum of 10 times the bar diameter away from each bar end. Thus, the bar's length-to-diameter ratio must be at least 20 for the stress wave to be effectively unidirectional. The Kolsky bar should be at least twice the striker length to prevent wave overlap at the strain gauge. Its length-to-diameter ratio should be within 40−150, aligning with one-dimensional elastic wave theory. This ratio ensures uniform axial stress distribution across the bar's cross-section and prevents wave overlap [31−33]. The input and output bars have same diameter of 20 mm with 1500 mm and 2000 mm in length, respectively. The input and output bar have the length-to-diameter as 57 and 100 to avoid the overlapping in the bar signals and disturbance. The input bar and output have been threatened on the gripping ends have a length of 20 mm with 10 mm diameter to holding the tensile specimen, see Fig. 6a. The shoulder used in the present investigation have 20 mm in length and outer diameter with 13 mm inner diameter, see Fig. 6a. The momentum bar and striker bar also have same diameter of 20 mm with different lengths of 1350 and 300 mm, respectively. The schematic of different cylindrical bars with their dimension has been shown in Fig. 6a. In additions, the actual arrangement of the bar components has been shown in Fig. 6b. The schematic diagram of tensile specimen and real specimen used for dynamic loading condition with geometrical configuration (all dimension in mm) has been shown in Fig. 6c. The yield strength of the bar material should exceed the maximum stress achievable in the specimen under dynamic tensile strength. This ensures that the stress induced in the bar remains comfortably within realistic elastic limits. Additionally, the bar materials must possess sufficient yield strength and hardness. This enables the specimen to undergo high strain rates without experiencing yielding. The quasi-static tensile test has been performed on the Steel 4340 dumbbell shaped specimen to determine the mechanical properties. The yield strength (corresponding to 0.2% of strain) and ultimate strength obtained as the 545 and 775 MPa with 17.3% elongation at break. The Young's modulus of elasticity (E_b) and density obtained as 210 GPa and 7936 kg/m^3, respectively. The wave velocity within the bar calculated as the $C_o = \sqrt{E_b/\rho_o} = 5144$ m/s. To prevent any inconsistency in wave impedance, it is essential for the input bar, output bar, and striker bar to share the same material properties and diameter.

5. DATA ACQUISITION AND RECORDING SYSTEM

An efficient and precise data acquisition system is very essential for collecting data during dynamic loading scenarios. The data recorded on the surface of input and output bars in the strain-time format by using the strain gauges mounted over the surfaces of the bars. The immediate elastic strain recorded on the surfaces of both the input and output bars holds significant importance for tasks such as calibration, data analysis, and evaluating the material's mechanical properties. The duration and magnitude of the strain pulse are documented in the microseconds and microstrains, respectively. To facilitate data acquisition, major equipment such as the strain gauge, Wheatstone bridge, Strain conditioner, oscilloscope, and processing controller are indispensable. It's imperative that this equipment possesses the capability to effectively capture data under conditions of high-speed loading. The DAQS records the strain waves at a sample rate of 1 million sample per second with total 4 second recording duration by using the LAB View software program. The triggering for recording set on the channel 1 at trigger level 0.2 volt for both channels. We used the half Wheatstone bridge configuration for better, accurate, and errorless results.

5.1. Strain gauge and Wheatstone Bridge

In SHPB (Split Hopkinson Pressure Bar) experiments, strain gauges have evolved into a standard and essential technique for measuring bar strains worked on the principle of electrical conductance to convert deformation or strain into changes in electrical resistance. Their adaptability is remarkable, stemming from factors such as their compact size, versatility in applications, and straightforward installation process. The deformation in the specimen resulting modification in electrical resistance, thereby generating an electrical output signal in voltage-time output. This signal is proportionate to the strain occurring in the specimen under examination. Their efficacy is so important when dealing with high-speed loading conditions, demanding equipment capable of capturing data accurately under such circumstances. The FLAB-3-11 type electrical resistance strain gauges used for the developed SHPB-T setup were manufactured by Tokyo Measuring Instruments Lab. The typical strain gauges had a 3 mm gauge length, 2.08 ±
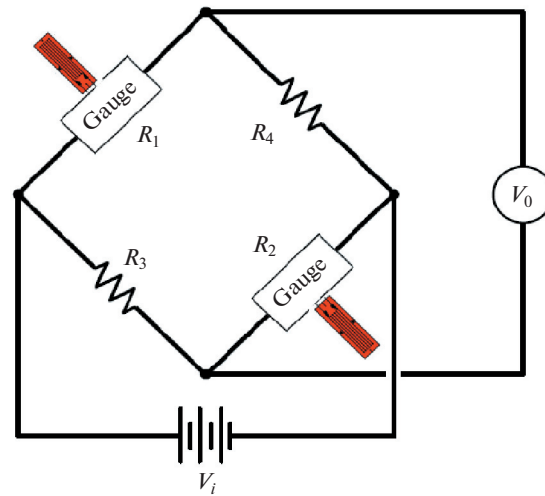
Fig. 7. Strain gauge connected in Wheatstone bridge.

1.0%-gauge factor, and $120 \pm 0.3\%$ Ω nominal gauge resistance. The bar's axial deformation (compression or tension) is directly correlates with the variation in strain gauge resistance (ΔR). The connection between the bar's deformation and the strain gauge resistance change is influenced by the strain gage factor (GF) by the following relation.

$$GF = \frac{\Delta R/R}{\Delta L/L}. \tag{8}$$

The ΔR and R represents the change in the resistance and nominal resistance of the strain gauge, respectively. Similarly, ΔL and L are the change in the gauge length and initial gauge length, respectively.

The Wheatstone bridge circuit capable to detects very small voltage changes resulting from variation in the strain gauge resistance generated due to deformation in the structural element. It comprising of four resistors, it can be configured in quarter, half, or full bridge setups. Our application employed the half bridge arrangement with two symmetrically placed strain gauges at the input and output bar surfaces.

Two strain gauges were linked to opposite sides of a Wheatstone bridge (refer to Fig. 7). Here, $R_1 = R_2 = R_{sg}$, where R_{sg} represents the nominal resistance of the strain gauge. On each bar surface, a pair of strain gauges were attached to resistors R_3 and R_4 in a way that $R_1 = R_3$ and $R_2 = R_4$, aimed at balancing the Wheatstone bridge. By connecting the strain gauges in a half-bridge setup, potential bending effects in the bar were eliminated. This configuration not only doubled the sensitivity of the Wheatstone bridge by employing two strain gauges for a given location's output but also eradicated the non-linear impacts associated with using just one active strain gauge connected in quarter configuration. The half-bridge arrangement od strain gauge specifically responded to longitudinal bar strain components while cancelling out strains resulting from bending. The Wheatstone bridge's output (V_o) and excitation voltage (V_i) can be related to the strain gauge resistance change (ΔR) through the following relationship,

$$V_o = \frac{1}{2}\frac{\Delta R}{R_{sg}}V_i. \tag{9}$$

In the half bridge configuration, the strain (ε) in bar and output voltage (V_o) are correlated as follows;

$$\varepsilon = \frac{2V_o}{(GF)V_i}. \tag{10}$$

5.2. Conditioner, Oscilloscope and Controller

The Wheatstone bridge produces a low amplitude output voltage, typically in the millivolt range. To enhance the recording process, a signal amplifier is essential to magnify and refine the weak voltage signal. In this study, a Digital Strain conditioner was utilized for quarter and half bridge setups. This conditioner, depicted in Fig. 8a, features a channel selector switch. It's programmed for two strain gauge resis-
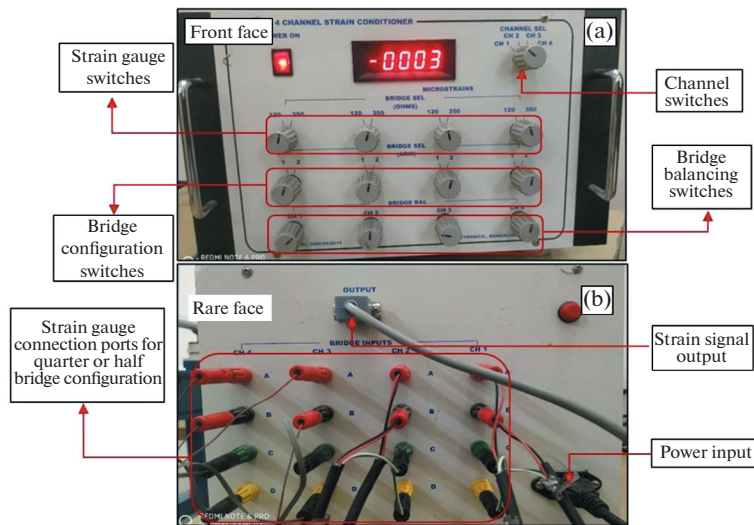
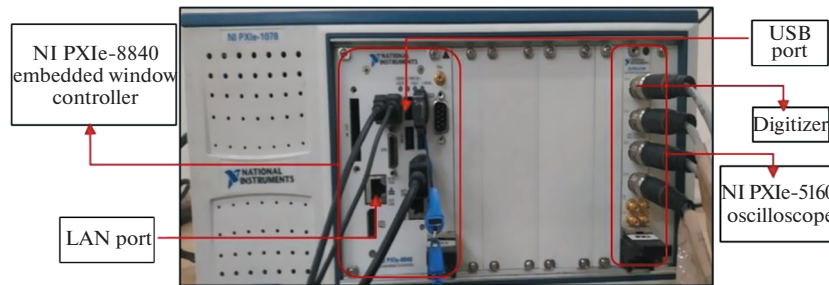**Fig. 8.** Digital Strain Conditioner: a) Front face; b) Rare_race.

Fig. 9. Oscilloscope and controller.

tance values: 120 and 350 ohms, chosen via a two-way rotary switch, as shown in the same figure. This device operates on a $0-12$ Volt DC excitation power supply and encompasses 4 sets of bridge connections facilities. Each set is equipped with 4 terminals for strain gauge attachment, illustrated in Fig. 8b. Consequently, the Conditioner delivers a simultaneous output of 4 channels, each providing an analog output of ± 5 Volts, directly proportional to the strain applied.

The conditioner output was linked to the PXIe-5160 Express Oscilloscope (National Instrumentation's model, Fig. 9). This oscilloscope boasted a 1.25 Giga-Sample per/sec max sample rate, four input digitizers, 500 MHz max bandwidth, 10-bit resolution, and 2 GB on board memory. Input signal employed with the BNC connectors. The oscilloscope's LabVIEW software-controlled output was displayed as an X-Y graph, with the vertical axis indicating output voltage within ± 5.0 volts and the horizontal axis representing time in increments of 1 nanosecond. Sample rate was adaptable through software, initially set at 1 million samples per second for calibration. Control of the experiment was managed by the NI PXIe-8840 embedded controller, operating with LabVIEW on a 2.7 GHz, Dual-Core Intel Core i5-4400E processor, backed by 8 GB RAM and featuring multiple communication ports including USB, LAN, and Ethernet (Fig. 9).

6. CALIBRATION OF TENSILE SHPB APPARATUS

After the development of the SHPB-T system, it is essential to conduct calibration on the setup before commencing with the experimentation phase. The calibration process for the SHPB test arrangement holds significant importance as a preliminary stage preceding dynamic material testing. Its primary purpose is to minimize the potential measurement uncertainties and confine errors within an acceptable limit. The tests were conducted to calibrate the newly developed setup using various striker impact veloc-

ities. This was done to create different loading conditions in the absence of a specimen. Te trials tests have been performed with the shoulder in absence of specimen. The shoulder act as a medium between the incident bar and the transmission bar have the identical mechanical impedance to the bars. This similarity in impedance enables near-complete transmission of waves. The strain pulse that travels through the transmission bar demonstrates as compressive in nature. However, the wave nature invert upon reaching the free end of the transmission bar. As a result, the shoulder plays a crucial role in generating tensile waves within the specimen located in the input bar.

6.1. Bar Length and Location of Strain Gauge

In the present experimental study, the presence of shoulder causes disturbances coming from the from reflected pulse from the bar-shoulder boundary was observed, see Fig. 12. The experimental observations made by the authors themselves, along with experiments conducted by other researchers, have consistently demonstrated that even after grinding the bars and shoulder surfaces, the wave pulse continues to reflect at the element boundaries due to a mismatch in mechanical impedance. These disruptions could potentially disrupt the primary wave signals and result in inaccuracies when determining the stress-strain curve [27, 34]. To prevent encountering such a scenario, varying lengths of pressure bars are commonly utilized. Typically, the length of the output bar is twice that of the input bar. Furthermore, when configuring the bar system, the placement of strain gauges is carefully selected to ensure unobstructed recording of wave pulses and to avert any interference with strain measurements.

The pulse generated by the shoulder and output bar interface causes disturbances with transmitted waves travelled through the specimen. If both the (input and output) bars have the same length, then the disturbance pulse and the tensile loading wave in input bar will reach simultaneously at the interface of the output bar and the shoulder, and this will lead to the over lapping of the disturbance pulse and tensile transmitted wave and hence the error in the determination of the data of the tensile transmitted wave occurred [34]. If the length of the input bar is more than the output bar, then the disturbance pulse generated by the shoulder will reach earlier at the interface and it will pass through the shoulder and the specimen as a compressive pulse, which will affect the results of the incident and reflected waves [34]. To avoid both situations, we can conclude that the length of the input bar should be less than the output bar. In this research, the input bar and the output bar lengths were 1500 mm and 2000 mm, respectively.

The compression loading pulse is generated in the bar when the striker bar impacts the output bar collinearly. This pulse then propagates towards the shoulder situated between the output bar and input bar. However, due to non-ideal contact between the output bar and shoulder, a portion of the incident pulse gets reflected into the output bar. This reflection occurs because the shoulder causes a mismatch in mechanical impedance. Because of this impedance mismatch, small amplitude signals with a tensile nature are generated in the output bar, see Fig. 12. Simultaneously, the incident pulse transmits into the input bar and subsequently reflects as a tensile pulse, see Fig. 12. This process results in the creation of a complex system of wave propagation within the input and output bars. Consequently, these wave signals interfere with each other, leading to various disturbances and interferences. To prevent the any disturbance and interference in the required output signals, it is necessary to determine the correct location of the strain gauges. The accuracy in selecting the positions of the strain gauges is demonstrated through the absence of any interference between disturbances and a transmitted pulse. To accomplish this purpose, the 4 strain gauges (SG) has been installed on the bar surfaces with 2 strain gauges in each bar, as shown in Fig. 10. The SG-1 mounted at 500 mm from the free end of the output bar and SG-2 placed at 80 mm form the output bar-shoulder contact interface, see Fig. 10. Similarly, the SG-3 placed at distance of 600 mm from shoulder-input bar interface and SG-4 placed at 450 mm form the free end of input bar, see Fig. 10. On the basis of experimental analysis, it was observed that the location of SG-2 in output bar and SG-3 in input bar found to be most suitable positions for the experimental studies. There is no mixing of the incident and reflected waves for 600 mm distance from the shoulder and input bar interference. It may therefore be concluded that the strain gauge should be placed at the input bar after the distance equal to the length of the striker measured from specimen and input bar interface. In this study, the data was collected at the centre of span of the input bar. These placements of the strain gauges ensure the accurate recording of output wave signals, free from any disturbance caused by shoulder applications.

6.2. Wave Characteristics

The characteristics of the stress wave generated through the SHPB system depends upon the bar alignment and striker bar impact velocity on incident bar. A good and proper alignment between striker and incident bar produces an analytically predictable trapezoidal profile of the incident pulse. When the striker
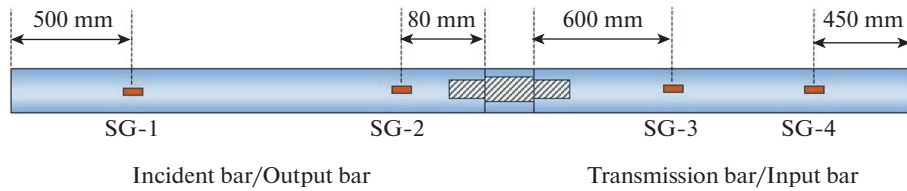
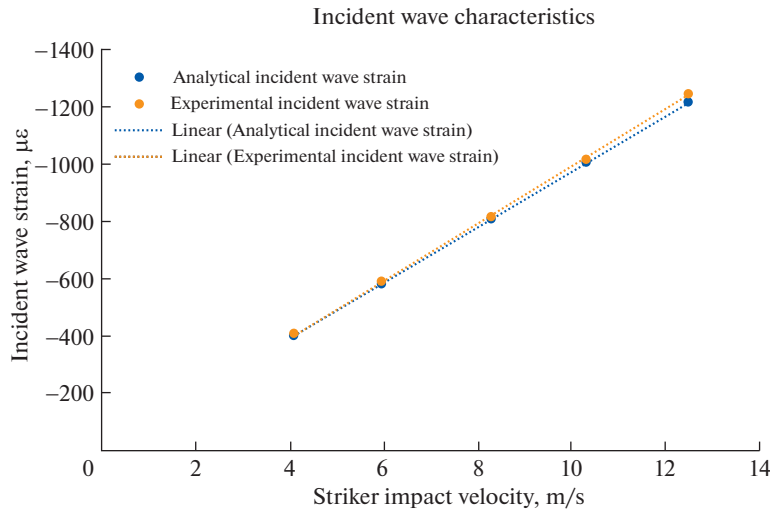**Fig. 10.** Location of strain gauges on the bars.

Fig. 11. Incident wave strain amplitude at varying striker impact velocity.

and incident bars have same diameter and same material properties, the stress and strain amplitude of the incident pulse depends upon the striking velocity through the following the equation;

$$\varepsilon_I = \frac{1}{2}\frac{V_{st}}{C_o}, \tag{11}$$

$$\sigma_I = \frac{1}{2}\rho_b C_o V_{st}, \tag{12}$$

where σ_I and ε_I are the stress and strain amplitude of the trapezoidal pulse in the incident bar used for the calibration purpose, V_{st} is the striker impact velocity, C_o is elastic bar wave speed of the bar material.

To validate the experimental incident wave characteristics with the analytical findings, the experiments were performed at varying striker impact velocities in the range of 4 to 14 m/s and the recorded incident wave characteristics at the SG-1 and SG-2 location has have been enlisted in Table 1. The data obtained during the calibration process described consistency in the output signals because of the variation in the incidence velocity. The wave velocity measured between SG-1 and SG-2 in different experimental loading. Three runs of the experiment were used and the resulting wave velocity obtained as 5122.6 m/s, 5141.38 and 5167.96 m/s. The average wave speed of the steel 4340 pressure bars is determined to be 5144 m/s. The density of bars can be calculated as 7936 kg/m³. From the wave speed relationship $C_o = \sqrt{E_b/\rho_o} = 5144$ m/s, the young's modulus of bar calculated as 210 GPa. The incident strain wave amplitude in incident bar is recorded at two location SG-1 and SG-1 to minimize the error. The experimentally recoded strain value at different impact velocities compared with the strain obtained from equation 1 analytically. The experimental, analytical, and % error in the wave amplitude has been listed in Table 1.

The striker impact velocity varied from 4 to 14 m/s to change the loading conditions in the bars and a comparative study of experimental and analytical incident bar strain has been carried out through curve fitting method, see Fig.12. The average experimental incident wave strain peak amplitude (Average of strain at SG-1 and SG-2) recorded at 4.1, 5.95, 8.3, 10.3, and 12.5 m/s striker impact velocity was −405, −588, −815, −1014, and −1243 micro-strain, respectively. It was observed −1.69, −1.76, −1.03, −1.36,
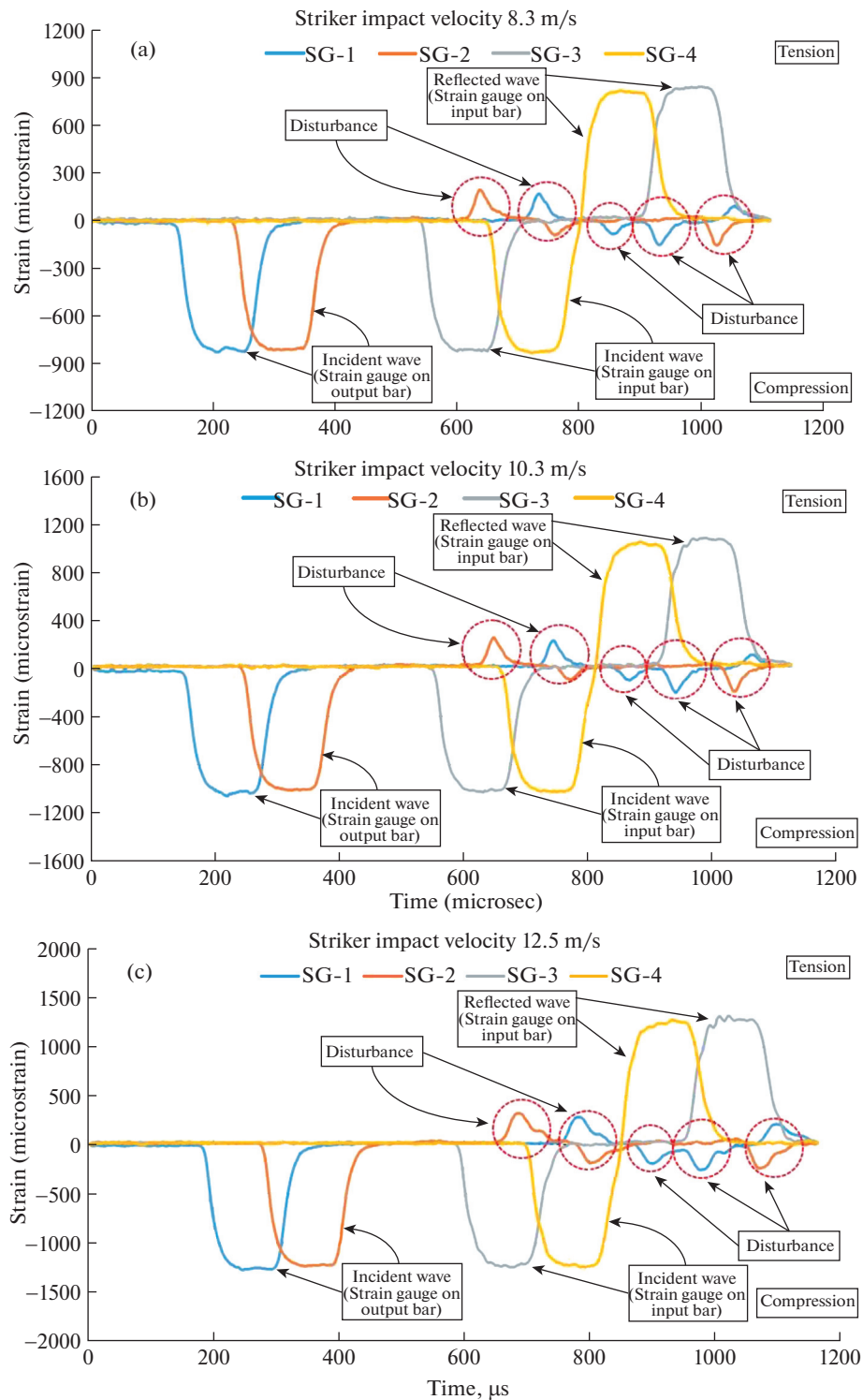
Fig. 12. (a) Strain signals recorded with shoulder by strain gauges at 8.3 m s^{-1} impact velocity. (b) Strain signal recorded with shoulder by strain gauges at 10.3 m s^{-1} impact velocity. (c). Strain signal recorded with shoulder by strain gauges at 12.5 m s^{-1} impact velocity.

and −2.37% error in the incident wave strain amplitude at the respective impact velocities. Here the negative sign indicates the compressive nature of the incident wave. The percentage error was found to be

Table 1. Incident Wave Characteristics at SG-1 and SG-2 Location in incident bar

Striker impact velocity m/s	Strain gauge location	Analytical incident strain με (microstrain)	Experimental incident strain με (microstrain)	Average experimental strain με (microstrain)	Error %	Average error %
4.10	SG-1	−398.52	−409.01	−405.24	−2.63	−1.69
	SG-2	−398.52	−401.46		−0.74	
5.95	SG-1	−578.34	−593.64	−588.52	−2.64	−1.76
	SG-2	−578.34	−583.40		−0.87	
8.30	SG-1	−806.77	−818.20	−815.08	−1.42	−1.03
	SG-2	−806.77	−811.96		−0.64	
10.30	SG-1	−1001.17	−1028.87	−1014.80	−2.77	−1.36
	SG-2	−1001.17	−1000.73		0.04	
12.50	SG-1	−1215.01	−1258.91	−1243.76	−3.61	−2.37
	SG-2	−1215.01	−1228.61		−1.12	

within 2.5% in the experimental results. Hence, on the basis of experimental results it has been concluded that the striker bar and incident bar were precisely aligned and collinear impact occurred.

After calibrating the striker bar and the incident bar, the alignment of the incident bar, shoulder, and transmission bars was accurately observed. This was achieved by conducting trials without specimens while adjusting the incidence velocity. Ideally, when the striker, incident, shoulder, and transmission bars are correctly aligned, the trapezoidal pulse recorded on the surfaces of the incident and transmission bars should exhibit nearly identical amplitude. Reflection of the pulse should be minimal or nonexistent under these optimal conditions [25]. Thus, the incident bar, shoulder, and transmission bar have been kept in proper face to face contact before performing the experiment, see Fig. 10. The incident strain pulse and transmission strain pulse recorded at SG-1, SG-2, SG-3, and SG-4 location with the help of strain gauge under 4.1, 5.95, 8.3, 10.3 and 12.5 m/s and the average peak incident and transmission bar strain amplitude obtained have been enlisted in Table 2. The recorded signal at 8.3, 10.3 and 12.5 m/s has been shown in Fig. 12 for the illustration. It has been observed that the presence of shoulder causes disturbances coming from pulse reflection from the bar-shoulder boundary surfaces. Hence, little reflected pulse at the bar-shoulder interface recorded due to non-ideal contact of the bar-shoulder at the interface resulting in the difference of mechanical impedance of shoulder and bars at the interface [34]. The percentage increment in the experimentally obtained strain value from the analytical strain values recorded at various location (SG-1, SG-2, SG-3, and SG-4) on incident and transmission bar at 4.1, 5.95, 8.3, 10.3 and 12.5 m/s striker impact velocities has been enlisted in Table 2. The maximum strain value recorded are 409.1, 593.64, 823.81, 1028.87, and 12.58.92 at the SG-1, SG-1, SG-4, SG-1, and SG-1 strain gauge location in bar corresponding to 4.1, 5.95, 8.3, 10.3 and 12.5 m/s impact velocity, respectively. There were a maximum 2.63, 2.64, 2.11, 2.77 and 3.62% increment in the experimental value as compared to the analytical calculation. Also, it can be observed that the average values of the recorded strain gauges have 1.80, 1.93, 1.43, 1.26 and 1.70% higher strain amplitude as compared to analytical values obtained from Fig. 12 corresponding to their striker impact velocities. This deviation in the experimental results from that of the ideal calculated results obtained from Eqn. 17 might have occurred due to some nominal misalignment of bars and shoulder, and due to difference in the mechanical impedance at the interfaces [34−36]. On the basis of experimental results, it has been observed there were less than 2% error was observed in the average peak strain in comparison to the analytical results. It has been concluded that the system is accurately aligned. In the absence of a specimen the striker, incident, shoulder, and transmission bars function as a single bar.

7. CONCLUSIONS

The output incident and transmitted wave signals obtained were found to be consistent with the striker bar impact velocity that was varied in the range 4−14 m/s. The elastic compressive wave developed in the incident bar was almost completely transferred to the transmission bar through the shoulder with minor

Table 2. Incident and transmission bar strain pulse amplitude error recorded at various locations

Striker impact velocity m/s	Bar	Strain gauge	Analytical strain με (microstrain)	Experimental strain με (microstrain)	Error %
4.1	Transmission/Input	SG-3	−398.52	−404.89	−1.60
		SG-4	−398.52	−407.35	−2.21
5.95	Transmission/Input	SG-3	−578.34	−590.66	−2.13
		SG-4	−578.34	−590.43	−2.09
8.3	Transmission/Input	SG-3	−806.77	−819.10	−1.53
		SG-4	−806.77	−823.81	−2.11
10.3	Transmission/Input	SG-3	−1001.17	−1011.94	−1.08
		SG-4	−1001.17	−1013.55	−1.24
12.5	Transmission/Input	SG-3	−1215.01	−1226.74	−0.97
		SG-4	−1215.01	−1228.26	−1.09

disturbance showing accuracy and preciseness of bar alignment system and parallelism of bar end faces. The elastic wave speed in the Steel 4340 bar observed as 5144 m/s. To avoid the overlapping of disturbance generated due to shoulder in the output bar, the length of output bar and input bar taken as 2000 and 1500 mm, respectively. Additionally, the location of SG-2 in output bar and SG-3 in the input bar are the most suitable location of the strain gauges to avoid the disturbance in the output results. The average experimental incident wave strain peak amplitude (Average of strain at SG-1 and SG-2) recorded at 4.1, 5.95, 8.3, 10.3, and 12.5 m/s striker impact velocity was −405, −588, −815, −1014, and −1243 microstrain, respectively. It was observed −1.69, −1.76, −1.03, −1.36, and −2.37% error in the incident wave strain amplitude at the respective impact velocities. The percentage error was found to be within 2.5% in the experimental results. Hence, on the basis of experimental results it has been concluded that the striker bar and incident bar were precisely aligned and collinear impact occurred. Similarly for the proper alignment of Striker, incident, shoulder, and transmission bar, the average values of the recorded strain gauges have 1.80, 1.93, 1.43, 1.26 and 1.70% higher strain amplitude as compared to analytical values corresponding to their striker impact velocities. On the basis of experimental results, it has been observed there were less than 2% error was observed in the average peak strain in comparison to the analytical results. Hence, it has been concluded that the system is accurately aligned such that in the absence of a specimen the striker, incident, shoulder, and transmission bars function as a single bar. It may be concluded that the developed SHPB-T setup has been well calibrated and could be suitably used to perform the further experiments on metals.

FUNDING

CONFLICT OF INTEREST

The authors of this work declare that they have no conflicts of interest.

DECLARATION

All authors have been confirming their approval for publication and declare no conflicts of interest among them.

REFERENCES

1. T. Bhujangrao, C. Froustey, E. Iriondo, et al., "Review of intermediate strain rate testing devices," Metals **10** (7), 894 (2020) .
https://doi.org/10.3390/met10070894

2. W.W. Chen and B. Song, *Split Hopkinson (Kolsky) Bar: Design, Testing and Applications* (Springer Science & Business Media, 2010).

3. F.W. Marrs, V.W. Manner, A.C. Burch, et al., "Sources of variation in drop-weight impact sensitivity testing of the explosive pentaerythritol tetranitrate," Ind. Eng. Chem. Res. **60** (13), 5024−5033 (2021). https://doi.org/10.1021/acs.iecr.0c06294

4. G. T. Gray III, "Classic split Hopkinson pressure bar testing," in *ASM Handbook*, Vol. 8: *Mechanical Testing and Evaluation*, Ed. by H. Kuhn and D. Medlin (ASM Int., 2000), pp. 462−476. https://doi.org/10.31399/asm.hb.v08.a0003296

5. W. Zhang, P. Hao, Y. Liu, and X. Shu, "Determination of the dynamic response of Q345 steel materials by using SHPB," Proc. Eng. **24**, 773−777 (2011). https://doi.org/10.1016/j.proeng.2011.11.2735

6. S. Tanimura, H. Hayashi, T. Yamamoto, and K. Mimura, "Dynamic tensile properties of steels and aluminum alloys for a wide range of strain rates and strain," J. Solid Mech. Mater. Eng. **3** (12), 1263−1273 (2009). https://doi.org/10.1299/jmmp.3.1263

7. A. Rajput and M. A. Iqbal, "Ballistic performance of plain, reinforced and pre-stressed concrete slabs under normal impact by an ogival-nosed projectile," Int. J. Impact Eng. **110**, 57−71 (2017). https://doi.org/10.1016/j.ijimpeng.2017.03.008

8. M. A. Iqbal, A. Rajput, and N. K. Gupta, "Performance of prestressed concrete targets against projectile impact," Int. J. Impact Eng. **110**, 15−25 (2017). https://doi.org/10.1016/j.ijimpeng.2016.11.015

9. A. Rajput, M. A. Iqbal, and C. Wu, "Prestressed concrete targets under high rate of loading," Int. J. Protect. Struct. **9** (3), 362−376 (2018). https://doi.org/10.1177/2041419618763933

10. A. Rajput, M. A. Iqbal, and N. K. Gupta, "Ballistic performances of concrete targets subjected to long projectile impact," Thin-Walled Struct. **126**, 171−181 (2018). https://doi.org/10.1016/j.tws.2017.01.021

11. N. Kojima, H. Hayashi, T. Yamamoto, et al., "Dynamic tensile properties of iron and steels for a wide range of strain rates and strain," Int. J. Modern Phys B. **22** (09n11), 1255−1262 (2008). https://doi.org/10.1142/S0217979208046621

12. M. M. Khan and M. A. Iqbal, "Dynamic response of concrete subjected to high rate of loading: a parametric study," Mech. Solids. **58** (4), 1378−1394 (2023). https://doi.org/10.3103/S0025654423600915

13. J. Hopkinson, "On the rupture of iron wire by a blow," Proc. Literary Phil. Soc. Manchester **1**, 40−45 (1872).

14. J. Hopkinson, "On the rupture of iron wire by a blow 1872 Article 38," in *Original Papers-by the Late John Hopkinson* (1901), pp. 316−320.

15. B. Hopkinson, "X. A method of measuring the pressure produced in the detonation of high, explosives or by the impact of bullets," Phil. Trans. Roy. Soc. Lond. Ser. A **213** (497−508), 437−456 (1914). https://doi.org/10.1098/rsta.1914.0010

16. R. M. Davies "A critical study of the Hopkinson pressure bar," Phil. Trans. Roy. Soc. Lond. Ser. A **240** (821), 375−457 (1948). https://doi.org/10.1098/rsta.1948.0001

17. H. Kolsky "An investigation of the mechanical properties of materials at very high rates of loading," Proc. Phys. Soc. B **62**, 676 (1949). https://doi.org/10.1088/0370-1301/62/11/302

18. J. M. Krafft, A. M. Sullivan, and C. F. Tipper, "The effect of static and dynamic loading and temperature on the yield stress of iron and mild steel in compression," Proc. Roy. Soc. Lond. Ser. A **221** (1144), 114−127 (1954). https://doi.org/10.1098/rspa.1954.0009

19. J. Harding, E.O. Wood, and J.D. Campbell "Tensile testing of materials at impact rates of strain," J. Mech. Eng. Sci. **2** (2), 88−96 (1960). https://doi.org/10.1243/JMES_JOUR_1960_002_016_02

20. F. E. Hauser, "Techniques for measuring stress-strain relations at high strain rates," Exp. Mech. **6** (8), 395−402 (1966). https://doi.org/10.1007/BF02326284

21. J. Duffy, J. D. Campbell, and R. H. Hawley, "On the use of a torsional split Hopkinson bar to study rate effects in 1100-0 aluminum" J. Appl. Mech. **38** (1), 83−91 (1971). https://doi.org/10.1115/1.3408771

22. U. S. Lindholm and L. M. Yeakley, "High strain-rate testing: tension and compression," Exp. Mech. **8** (1), 1−9 (1968). https://doi.org/10.1007/BF02326244

23. R. A. Frantz Jr. and J. Duffy, "The dynamic stress-strain behavior in torsion of 1100-0 aluminum subjected to a sharp increase in strain rate," J. Appl. Mechs. **39** (4), 939−945 (1972). https://doi.org/10.1115/1.3422895

24. T. Nicholas "Tensile testing of materials at high rates of strain," Exp. Mech. **21** (5), 177−185 (1981). https://doi.org/10.1007/BF02326644

25. B. Song, K. Connelly, J. Korellis, et al., "Improved Kolsky-bar design for mechanical characterization of materials at high strain rates," Meas. Sci. Technol. **20** (11), 115701 (2009). https://doi.org/10.1088/0957-0233/20/11/115701

26. R. Govender, M. Kariem, D. Ruan, et al., "Towards standardising SHPB testing-A Round Robin exercise," EPJ Web Conf. **183**, 02027 (2018). https://doi.org/10.1051/epjconf/201818302027

27. R. Gerlach, Ch. Kettenbeil, and N. Petrinic, "A new split Hopkinson tensile bar design," Int. J. Impact Eng. **50**, 63−67 (2012). https://doi.org/10.1016/j.ijimpeng.2012.08.004

28. D. Mohr and G. Gary, "M-Shaped specimen for the high-strain rate tensile testing using a split Hopkinson pressure bar apparatus," Exp. Mech. **47**, 681−692 (2007). https://doi.org/10.1007/s11340-007-9035-y

29. G. H. Staab and A. Gilat, "A direct-tension split Hopkinson bar for high strain-rate testing," Exp. Mech. **31** (3), 232−235(1991). https://doi.org/10.1007/BF02326065

30. K. Ogawa, "Impact-tension compression test by using a split-Hopkinson bar," Exp. Mech. **24** (2), 81−86 (1984). https://doi.org/10.1007/BF02324987

31. U. S. Lindholm, "Some experiments with the split hopkinson pressure bar," J. Mech. Phys. Solids. **12** (5), 317−335 (1964). https://doi.org/10.1016/0022-5096(64)90028-6

32. L. Wang, *Foundations of Stress Waves* (Elsevier, 2011).

33. M. Hassan and K. Wille, "Experimental impact analysis on ultra-highperformance concrete (UHPC) for achieving stress equilibrium (SE) and constant strain rate (CSR) in Split Hopkinson pressure bar (SHPB) using pulse shaping technique," Construct. Build. Mater. **30** (144) 747−757 (2017). https://doi.org/10.1016/j.conbuildmat.2017.03.185

34. R. Panowicz and J. Janiszewski, "Tensile split Hopkinson bar technique: numerical analysis of the problem of wave disturbance and specimen geometry selection," Metrol. Meas. Syst. **23** (3), 425−436 (2016). https://doi.org/10.1515/mms-2016-0027

35. M.A. Kariem, J.H. Beynon, and D. Ruan "Misalignment effect in the split Hopkinson pressure bar technique," Int. J. Impact Eng. **1** (47) 60−70 (2012). https://doi.org/10.1016/j.ijimpeng.2012.03.006

36. M. M. Khan and M. A. Iqbal, "Design, development, and calibration of split Hopkinson pressure bar system for dynamic material characterization of concrete," Int. J. Protect. Struct. 20414196231155947 (2023). https://doi.org/10.1177/20414196231155947

Publisher's Note. Allerton Press remains neutral with regard to jurisdictional claims in published maps and institutional affiliations.